ACS OMEGA

http://pubs.acs.org/journal/acsodf

Article

Entropy Change Characteristics of the $LiNi_{0.5}Mn_{1.5}O_4$ Cathode Material for Lithium-Ion Batteries

Jing Mao,* Peng Zhang, Xin Liu, Yanxia Liu, Guosheng Shao, and Kehua Dai*

Cite This: *ACS Omega* 2020, 5, 4109−4114

Read Online

ACCESS | Metrics & More | Article Recommendations

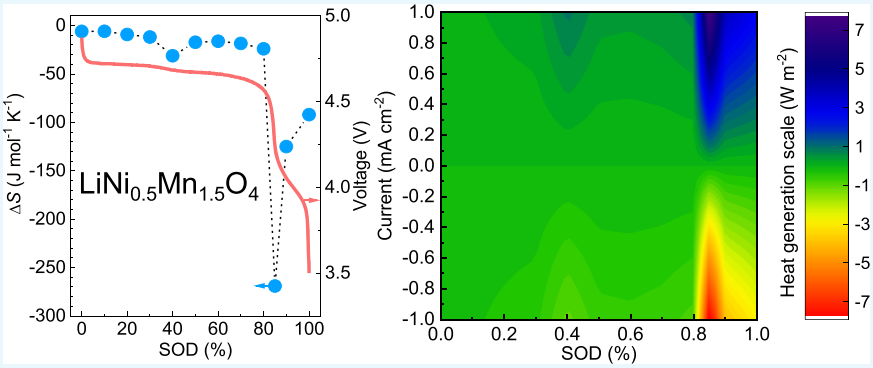

ABSTRACT: Lithium-ion batteries are widely used in the field of new energy vehicles and energy storage. Understanding the electrode reaction of lithium-ion batteries is the key to improve their cycle life and safety. Direct measurement of thermodynamic data of the electrode reaction is a practical, economical, and nondestructive method for electrode characterization. In this paper, the open-circuit voltage of the $LiNi_{0.5}Mn_{1.5}O_4$/Li half-cell is measured at different discharge states and different temperatures. The dE/dT−SOD (state of discharge) relation curves are fitted linearly by the least square method, and the entropy change values of different SODs are calculated. Finally, the Gibbs free energy and enthalpy change of different SODs are obtained. The electrode reaction of $LiNi_{0.5}Mn_{1.5}O_4$ in different SODs was discussed by the entropy change in different SODs. According to the evolution trend of ΔS, the lithium intercalation reaction of $LiNi_{0.5}Mn_{1.5}O_4$ may be a single-phase solid solution reaction rather than a two-phase reaction. Finally, the reversible heat generation at different current values and SODs are calculated.

1. INTRODUCTION

Lithium-ion batteries are widely used in the field of new energy vehicles and energy storage.[1,2] The cycle life and safety of lithium-ion batteries are the most concerned issues.[3−5] In order to improve the cycle life, it is necessary to understand the mechanism of the electrode reaction and decay.[6,7] For safety concerns, one of the important issues is improving the battery design.[8] The design improvement requires better understanding of the heat generation behavior of batteries in charging and discharging, which is determined by the characteristics of the electrode material itself.[9−11]

Currently, many in situ characterization methods are used to understand the electrode reaction and decay mechanism of lithium-ion batteries.[12−16] However, these characterization methods often need to be combined with specially designed cell models and electrode materials with special morphology, which is not convenient in many cases. Therefore, direct measurement of the thermodynamic data of the electrode reaction is a practical and economic means of electrode characterization, which is often ignored by material researchers.[17] The measurement of electrode reaction and thermodynamic parameters is carried out in the half-cell or the full-cell. The whole measurement process has a little disturbance to the battery, so it can be considered to be a nondestructive in situ battery detection method. In other words, commercial lithium-ion batteries can be detected in situ without damage. In addition, thermodynamic characterization can be used not only to characterize the thermal properties of various electrode materials but also to characterize the structural changes and electrode reactions in the process of charging and discharging.[18] It is a powerful method to study the cycle life and safety of batteries.[9,19]

The three most important thermodynamic parameters of the electrode reaction are Gibbs free energy G, entropy S, and enthalpy H. The change in Gibbs free energy ΔG is the maximum work of the battery. The change in lattice order is

Received: November 7, 2019
Accepted: January 31, 2020
Published: February 20, 2020

https://dx.doi.org/10.1021/acsomega.9b03794
ACS Omega 2020, 5, 4109−4114

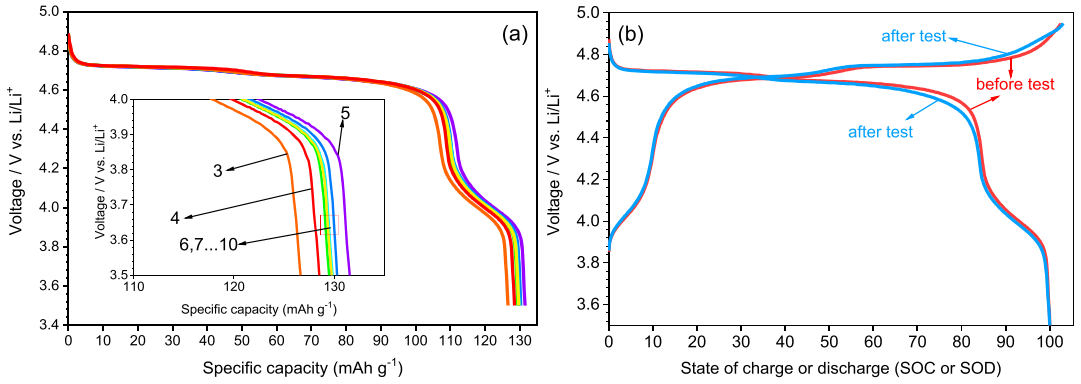

Figure 1. (a) Precycling voltage profiles from the third to tenth cycle; (b) voltage profiles before and after the OCV test for the $LiNi_{0.5}Mn_{1.5}O_4$/Li half-cell at 0.1 C, 20 °C.

characterized by the change in entropy ΔS. The enthalpy change ΔH is the reaction heat of the electrochemical reaction. These three parameters can be measured by electrochemical tests and eqs 1−3[20]

$$\Delta G = -nFE \tag{1}$$

$$\Delta S = nF\left(\frac{\partial E}{\partial T}\right)_P \tag{2}$$

$$\Delta H = \Delta G + T\Delta S = nF\left[T\left(\frac{\partial E}{\partial T}\right)_P - E\right] \tag{3}$$

where n is the number of electrons transfer per formula, F is the Faraday constant, E is the standard electromotive force [also known as open-circuit potential (OCV)] of the battery reaction, T is the temperature, and P is the pressure.

Item $(\partial E/\partial T)_P$, here referred to dE/dT, is determined by measuring the OCV of the electrochemical cell at different temperatures. Ideally, the cell needs to be relaxed for a period of time before the open-circuit voltage is measured to reach equilibrium. The entropy change in the electrochemical reaction can be obtained by measuring the change in open-circuit voltage at different temperatures and calculated using eq 2.[21] The increase or decrease in entropy means the decrease or increase in the degree of order of the lithium ion in the lattice, respectively. More importantly, the entropy change can also affect the thermal behavior of electrochemical reaction and then change the temperature of the battery, which greatly affects the performance of lithium-ion batteries.[9]

The total heat generation of the Li-ion battery can be calculated using eq 4[22]

$$Q_{total} = Q_{irreversible} + Q_{reversible} = -I^2R_i - T\Delta S\frac{I}{nF} \tag{4}$$

where I is the current value (the discharge current is determined to be negative here), R_i is the internal resistance of the battery, and ΔS is the entropy change. Negative Q means exothermic reaction in which heat is transferred from the battery. On the contrary, positive Q indicates an endothermic reaction. $Q_{irreversible}$ is always negative and only related to current and internal resistance. The positivity and negativity of $Q_{reversible}$ depend on the symbol of ΔS and current.[23] The sum of $Q_{irreversible}$ and $Q_{reversible}$ determines the symbol and size of Q_{total}, that is, the total amount of heat generated by the battery. For example, when ΔS is negative and I is negative in the discharge process, $-I^2R_i$ and $-T\Delta SI/nF$ are both negative values and Q_{total} is negative. In the charging process, I is positive, so $-T\Delta SI/nF$ is positive and $-I^2R_i$ is negative; thus, the positive and negative symbols of Q_{total} are determined by the larger absolute values of the two items.

In the process of charging and discharging, the concentration of the lithium ion in the solid phase of the electrode material is dynamic. According to eq 2, ΔS is a state function independent of the process, that is to say, it is not affected by the charging and discharging process and only changes with the concentration of the lithium ion. The relationship between them can be expressed by the entropy change curve. Currently, the entropy curves of many electrode materials and full-cells have been reported, including Li_xTiS_2,[24] $LiMn_2O_4$,[25] $LiCoO_2$,[24] $Li_xV_2O_5$,[26] graphite,[27] and so forth. With these basic physical chemistry parameters, people can build a more accurate thermoelectric-coupled modeling,[28] so as to realize the accurate prediction and simulation of the electrochemical performance and thermal behavior of lithium-ion batteries.[29−32]

$LiNi_{0.5}Mn_{1.5}O_4$ is a typical high-voltage cathode material with a voltage plateau as high as 4.7 V.[33,34] This material has a three-dimensional lithium-ion diffusion path and an excellent intrinsic rate performance.[35,36] In addition, it has been found that there may be a two-phase coexistence region and phase transition region in the voltage plateau, which can be attributed to the change in the degree of order caused by the rearrangement of Ni and Mn transition metals in the sublattice.[37] However, in full-cell applications, it has been found that the battery capacity decays faster than the commercial standard.[38] The capacity fading may be due to (1) the increase in interface impedance caused by the oxidation and decomposition of an electrolyte; (2) the loss of the active material caused by the dissolution of the transition metal. In addition, the stress caused by the crystal phase transformation during the lithium removal from the positive electrode may also cause capacity decay.[39] The electrochemical thermodynamic parameters are very sensitive to the phase transition, which is helpful to analyze the crystal phase transition when the cathode is deintercalated with lithium and to clarify the mechanism of smooth phase transition by doping element modification. As of now, there is no report available on the entropy change in $LiNi_{0.5}Mn_{1.5}O_4$. In this paper, we study the entropy change characteristics of $LiNi_{0.5}Mn_{1.5}O_4$/Li half-cell in different states of discharge (SODs).

https://dx.doi.org/10.1021/acsomega.9b03794
ACS Omega 2020, 5, 4109−4114

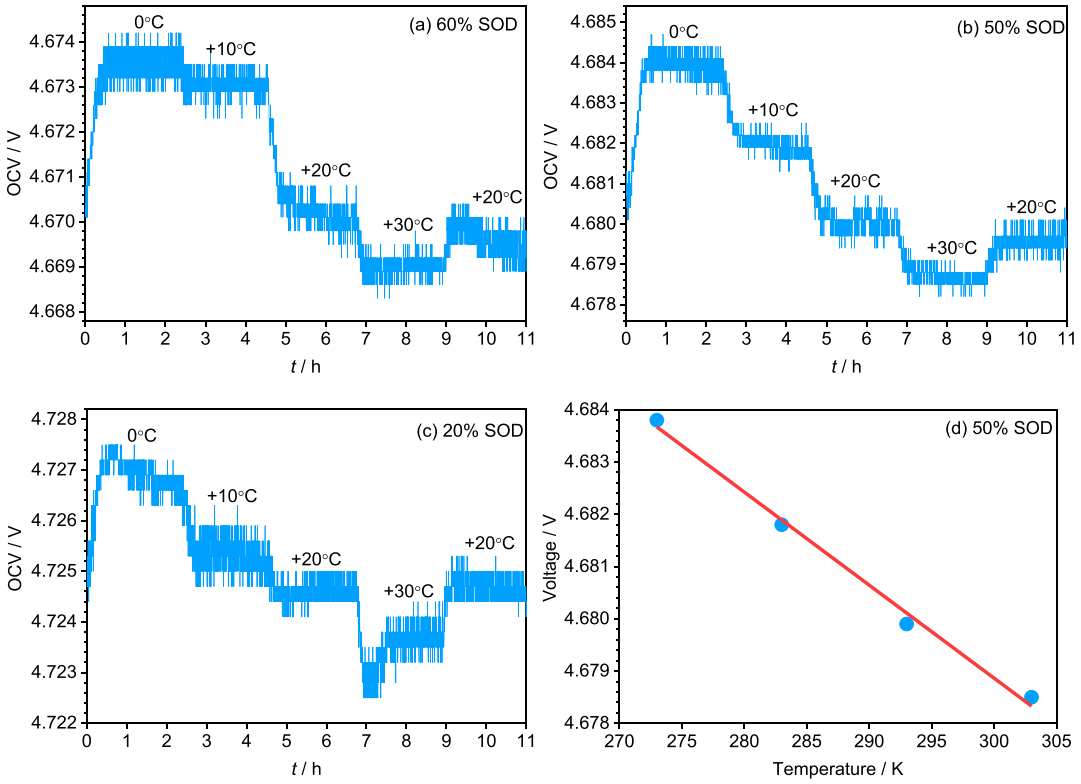

Figure 2. Potentiometric measurement (OCV vs time) for the $LiNi_{0.5}Mn_{1.5}O_4$/Li half-cell. (a) 60% SOD; (b) 50% SOD; and (c) 20% SOD. (d) Corresponding linear fitting (OCV vs temperature) at 50% SOD.

Table 1. Summary of Data for the $LiNi_{0.5}Mn_{1.5}O_4$/Li Half-Cell at Different SODs at 20 °C

SOD (%)	OCV/20 °C	dE/dT/mV K^{-1}	ΔS/J K^{-1} mol^{-1}	ΔG/kJ mol^{-1}	ΔH/kJ mol^{-1}
0	4.7336	−0.06	−6	−456.79	−458.548
10	4.7309	−0.061	−5.9	−456.53	−458.258
20	4.7251	−0.095	−9.2	−455.97	−458.665
30	4.7248	−0.123	−11.8	−455.94	−459.397
40	4.7184	−0.324	−31.2	−455.32	−464.461
50	4.6806	−0.178	−17.2	−451.67	−456.709
60	4.6742	−0.168	−16.2	−451.06	−455.806
70	4.6681	−0.191	−18.4	−450.47	−455.861
80	4.6589	−0.249	−24	−449.58	−456.612
85	4.4763	−2.788	−269	−431.96	−510.777
90	4.1264	−1.297	−125	−398.19	−434.815
100	3.7273	−0.954	−92	−359.68	−386.636

2. RESULTS AND DISCUSSION

Figure 1a shows the voltage profile of the $LiNi_{0.5}Mn_{1.5}O_4$/Li half-cell from the third to tenth cycle in the precycle stage at 0.1 C. It can be seen that after 10 cycles of precycling, the interface of the electrode is gradually stable. In particular, the discharge curve of the 4.7 V plateau is highly coincident, which indicates that the battery is stable, and the next step of thermodynamic parameter measurements can be carried out. It can be seen from the figure that the discharge capacity of the 4.7 V high-voltage plateau is about 115 mA h g^{-1}, accounting for 80% of the total discharge capacity, which is also the focus of this paper (compared with a 4 V slope stage).

The SOD may change slightly after the OCV test. Thus, if the cell is discharged to the next specific capacity point directly, the actual SOD may be different with the targeted point. In addition, the SOD cannot be adjusted by potential because of the very flat plateau before 80% SOD, which leads to a big capacity change with a small potential change, and an unacceptable SOD error. To obtain accurate SODs, the cell is fully charged and discharged to target SOD after every OCV tests. Figure 1b shows the charge−discharge curve of $LiNi_{0.5}Mn_{1.5}O_4$/Li half-cell before and after the OCV test. The curve basically coincides with each other, indicating that the battery and the electrode material structure are both stable in the whole test process. This suggests that the above test procedure is meaningful. The open-circuit voltage and temperature curves measured at steady state reflect the intrinsic thermodynamic characteristics of $LiNi_{0.5}Mn_{1.5}O_4$.

Figure 2a−c shows the open-circuit voltage versus time curves measured at 60, 50, and 20% SOD, respectively. Although the open-circuit voltage fluctuates slightly at the same temperature, the change in trend can be seen. As the temperature increases along 0, 10, 20, and 30 °C, the open-circuit voltage decreases in turn. The open-circuit voltage at

https://dx.doi.org/10.1021/acsomega.9b03794
ACS Omega 2020, 5, 4109−4114

the same temperature is taken as the middle value of the stable stage, and the obtained temperature versus open-circuit voltage curve (Figure 2d) meets the linear fitting condition, so $(\partial E/\partial T)_P$ can be obtained, and then, ΔS can be obtained according to eq 2.

Table 1 summarizes the open-circuit voltage, dE/dT, ΔS, ΔG, and ΔH values of the $LiNi_{0.5}Mn_{1.5}O_4$/Li half-cell for different SODs at 20 °C. Figures 3 and 4 show the open-circuit voltage curve and ΔS curve of the $LiNi_{0.5}Mn_{1.5}O_4$/Li half-cell for different SODs at 20 °C. It can be seen from Table 1 and Figure 4 that the ΔS value for 0−10% SOD (high-voltage lithium-deficient phase) is almost the same. It can be inferred that it conforms to the characteristics of first-order two-phase transformation, which is often accompanied by large volume change, resulting in large internal stress, particle fracture, and deterioration of cycle performance. In the range of 10−40% SOD, ΔS shows a slope change, which indicates that the reaction in this region is closer to the single-phase reaction of a solid solution rather than the two-phase reaction. The 40−60% SOD region is a transition region, indicating that there are new phases in the region, which is a multiphase coexistence region. In the 60−80% SOD range, ΔS also shows a slope change, indicating that the region is closer to the reaction mechanism of a single-phase solid solution. The OCV in the 80−100% SOD range is always unstable during measurement, and the calculation error of the mean value is large. However, it can also be seen qualitatively that the absolute value of ΔS in this area is large, and the volume changes greatly along with a huge amount of change in heat; therefore, this area corresponds to the $Mn^{4+} \rightarrow Mn^{3+}$ redox couple, rather than $Ni^{2+} \rightarrow Ni^{3+} \rightarrow Ni^{4+}$ redox. It has been reported that the lithium intercalation reaction is a two-phase reaction in $LiNi_{0.5}Mn_{1.5}O_4$, corresponding to the two-half plateau high-voltage regions.[37] In this paper, the intercalation is more like a single-phase solid solution reaction based on the evolution trend of ΔS.[40] The reason of the discrete conclusion with the previous report needs to be studied more in the future. One possible reason may be the content of Mn^{3+} in the samples, as it is reported that the increase in the degree of disorder by doping can make the ΔS get inclined to the slope.[41]

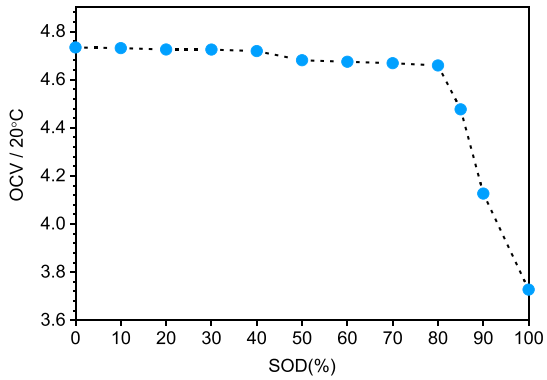

Figure 3. Open-circuit voltage vs SOD for the $LiNi_{0.5}Mn_{1.5}O_4$/Li half-cell at 20 °C.

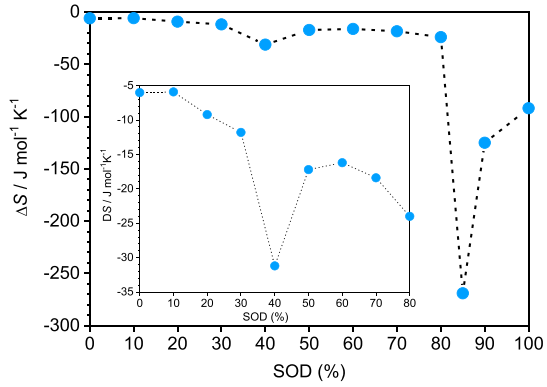

Figure 4. Entropy-SOD curve of the $LiNi_{0.5}Mn_{1.5}O_4$/Li half-cell.

Using open-circuit voltage data and eq 1, the value of ΔG under different SODs can be calculated, and then through eq 3, the value of ΔH can be obtained. Figure 5 shows ΔG (Figure 5a) and ΔH (Figure 5b) versus SOD curves of the $LiNi_{0.5}Mn_{1.5}O_4$/Li half-cell. The value of ΔH corresponds to the heat released by the electrochemical reaction of the battery. It is of great significance to study the heat generation and temperature change in the process of battery charging and discharging and then to carry out thermoelectric-coupled simulation and predictive management of the battery system.[22]

The reversible heat generation is calculated using eq 4, as shown in Figure 6. Because ΔS is always negative at all SODs, and I is negative in the discharge process, $-T\Delta SI/nF$ is negative, exhibiting the heating effect. In the charging process, I is positive, so $-T\Delta SI/nF$ is positive, exhibiting the cooling effect. The heating or cooling effect is rather strong from 80 to 90% SOD, for the absolute value of ΔS is large, and the structure changes severely in this range.

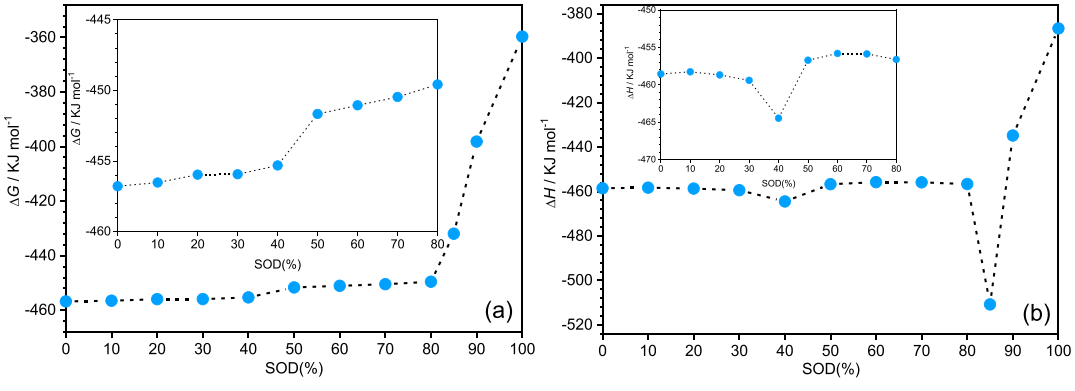

Figure 5. (a) ΔG and (b) ΔH vs SOD curves of the $LiNi_{0.5}Mn_{1.5}O_4$/Li half-cell.

https://dx.doi.org/10.1021/acsomega.9b03794
ACS Omega 2020, 5, 4109−4114

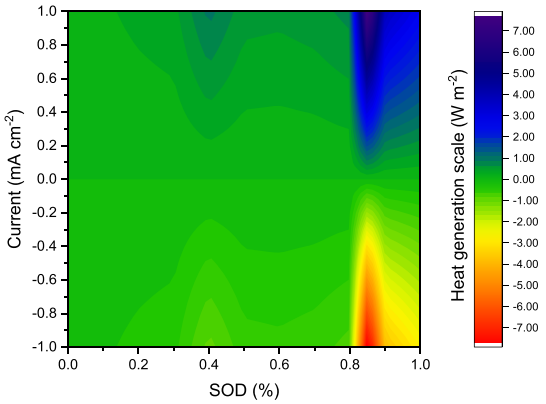

Figure 6. Reversible heat generation at different current values and SODs.

3. CONCLUSIONS

In this paper, the open-circuit voltage of the $LiNi_{0.5}Mn_{1.5}O_4$/Li half-cell at different discharge states and different temperatures is measured. As temperature increases, the open-circuit voltage decreases linearly in turn. The dE/dT−SOD relation curves are fitted by the least square method, and the entropy change values of different SODs are calculated based on the fitted values. The ΔS values do not change much in 0% to 80% SOD but change dramatically when the SOD is over 80%. Further, the Gibbs free energy and enthalpy change in different SODs are obtained. The electrode reaction of $LiNi_{0.5}Mn_{1.5}O_4$ was discussed by the entropy change in different SODs. According to the evolution trend of ΔS, the lithium intercalation reaction of $LiNi_{0.5}Mn_{1.5}O_4$ may be a single-phase solid solution reaction rather than a two-phase reaction. In this system, the reversible heat generation shows cooling and heating effect in the charging and discharging process, respectively.

4. METHODS

4.1. Material Preparation. A $LiNi_{0.5}Mn_{1.5}O_4$ material was prepared by a PVP gel combustion method. The detailed procedure can be found in our previous report.[42]

4.2. Electrode Preparation and Battery Assembly. The $LiNi_{0.5}Mn_{1.5}O_4$, an NMP solution in polyvinylidene fluoride, and conductive carbon black (super C) were mixed evenly according to a mass ratio of 8:1:1, doctor-bladed on aluminum foil, predried at 60 °C, transferred to a vacuum drying oven, and then dried overnight at 120 °C. The dry electrode pieces are punched into a circular electrode with a diameter of 12 mm, and the thickness is 15 μm. The CR2025 half-cells were fabricated with the $LiNi_{0.5}Mn_{1.5}O_4$ cathode, lithium foil anode, 1 mol L^{-1} $LiPF_6$ in 1:1 EC/DEC as the electrolyte, and Celgard 2400 as the separator in an argon-filled glovebox.

4.3. Electrochemical Test. The charge and discharge performance and open-circuit voltage of different SODs were examined by a LANHE CT2001A battery tester. The temperature is controlled by a programmable temperature-controlled incubator. Because the volume of the battery is very small compared with the incubator, we use the incubator temperature to represent the battery temperature. The SOD was adjusted by discharging at 0.1 C.

The test process consists of the following steps:

a Precycle: cycle at 20 °C, 0.03 C rate, voltage range 3.5−4.95 V for 10 cycles, and read battery capacity information after battery charging and discharging cycle curve is stable.

b Full charging: charge to 4.95 V at a constant current of 0.1 C, set as 100% state of charge, that is, 0% SOD.

c OCV test: first, balance the battery at 20 °C for 20 h and record the open-circuit voltage. Then, repeat the process at 0, 10, 20, 30, and 20 °C for 2 h at each step.

d Adjusting SOD: charge the cell fully and then discharge at 0.1 C to the target SOD in one step.

AUTHOR INFORMATION

Corresponding Authors

Jing Mao − *School of Materials Science and Engineering, Zhengzhou University, Zhengzhou 450001, China*; Email: maojing@zzu.edu.cn

Kehua Dai − *College of Chemistry, Tianjin Normal University, Tianjin 300387, China*; orcid.org/0000-0002-2292-7523; Email: daikehua@gmail.com

Authors

Peng Zhang − *School of Materials Science and Engineering, Zhengzhou University, Zhengzhou 450001, China*

Xin Liu − *School of Materials Science and Engineering, Zhengzhou University, Zhengzhou 450001, China*

Yanxia Liu − *Zhengzhou Institute of Emerging Industrial Technology, Zhengzhou 450001, China*

Guosheng Shao − *School of Materials Science and Engineering, Zhengzhou University, Zhengzhou 450001, China*; orcid.org/0000-0003-1498-7929

Complete contact information is available at: https://pubs.acs.org/10.1021/acsomega.9b03794

Notes

The authors declare no competing financial interest.

ACKNOWLEDGMENTS

This work was financially supported by the National Natural Science Foundation of China (51604244), Postdoctoral research grant in Henan province (001802003), and Science and Technology on Reliability Physics and Application of Electronic Component Laboratory open fund (ZHD201605).

REFERENCES

(1) Whittingham, M. S. Lithium batteries and cathode materials. *Chem. Rev.* **2004**, *104*, 4271−4302.

(2) Li, M.; Lu, J.; Chen, Z.; Amine, K. 30 years of lithium-ion batteries. *Adv. Mater.* **2018**, *30*, 1800561.

(3) Goodenough, J. B.; Kim, Y. Challenges for rechargeable li batteries. *Chem. Mater.* **2010**, *22*, 587−603.

(4) Tarascon, J.-M.; Armand, M. Issues and challenges facing rechargeable lithium batteries. *Nature* **2001**, *414*, 359−367.

(5) Kong, L.; Li, C.; Jiang, J.; Pecht, M. Li-ion battery fire hazards and safety strategies. *Energies* **2018**, *11*, 2191.

(6) Wu, Q.; Liu, Y.; Johnson, C. S.; Li, Y.; Dees, D. W.; Lu, W. Insight into the structural evolution of a high-voltage spinel for lithium-ion batteries. *Chem. Mater.* **2014**, *26*, 4750−4756.

(7) Ruan, Y.; Song, X.; Fu, Y.; Song, C.; Battaglia, V. Structural evolution and capacity degradation mechanism of $LiNi_{0.6}Mn_{0.2}Co_{0.2}O_2$ cathode materials. *J. Power Sources* **2018**, *400*, 539−548.

(8) Shui, L.; Chen, F.; Garg, A.; Peng, X.; Bao, N.; Zhang, J. Design optimization of battery pack enclosure for electric vehicle. *Struct. Multidiscip. Optim.* **2018**, *58*, 331−347.

https://dx.doi.org/10.1021/acsomega.9b03794
ACS Omega 2020, 5, 4109−4114

(9) Wang, S. Entropy and heat generation of lithium cells/batteries. *Chin. Phys. B* **2016**, *25*, 010509.
(10) Assat, G.; Glazier, S. L.; Delacourt, C.; Tarascon, J.-M. Probing the thermal effects of voltage hysteresis in anionic redox-based lithium-rich cathodes using isothermal calorimetry. *Nat. Energy* **2019**, *4*, 647−656.
(11) Liu, K.; Liu, Y.; Lin, D.; Pei, A.; Cui, Y. Materials for lithium-ion battery safety. *Sci. Adv.* **2018**, *4*, No. eaas9820.
(12) Bauer, S.; Biasi, L. d.; Glatthaar, S.; Toukam, L.; Gesswein, H.; Baumbach, T. In operando study of the high voltage spinel cathode material $LiNi_{0.5}Mn_{1.5}O_4$ using two dimensional full-field spectroscopic imaging of ni and mn. *Phys. Chem. Chem. Phys.* **2015**, *17*, 16388−16397.
(13) Qiao, R.; Wray, L. A.; Kim, J.-H.; Pieczonka, N. P. W.; Harris, S. J.; Yang, W. Direct experimental probe of the Ni(II)/Ni(III)/Ni(IV) redox evolution in $LiNi_{0.5}Mn_{1.5}O_4$ electrodes. *J. Phys. Chem. C* **2015**, *119*, 27228−27233.
(14) Ramdon, S.; Bhushan, B.; Nagpure, S. C. In situ electrochemical studies of lithium-ion battery cathodes using atomic force microscopy. *J. Power Sources* **2014**, *249*, 373−384.
(15) Dai, K.; Wu, J.; Zhuo, Z.; Li, Q.; Sallis, S.; Mao, J.; Ai, G.; Sun, C.; Li, Z.; Gent, W. E.; Chueh, W. C.; Chuang, Y.-d.; Zeng, R.; Shen, Z.-x.; Pan, F.; Yan, S.; Piper, L. F. J.; Hussain, Z.; Liu, G.; Yang, W. High reversibility of lattice oxygen redox quantified by direct bulk probes of both anionic and cationic redox reactions. *Joule* **2019**, *3*, 518−541.
(16) Qiao, R.; Dai, K.; Mao, J.; Weng, T.-C.; Sokaras, D.; Nordlund, D.; Song, X.; Battaglia, V. S.; Hussain, Z.; Liu, G.; Yang, W. Revealing and suppressing surface Mn(II) formation of $Na_{0.44}MnO_2$ electrodes for na-ion batteries. *Nano Energy* **2015**, *16*, 186−195.
(17) Thomas, K. E.; Bogatu, C.; Newman, J. Measurement of the entropy of reaction as a function of state of charge in doped and undoped lithium manganese oxide. *J. Electrochem. Soc.* **2001**, *148*, A570−A575.
(18) Yazami, R.; Reynier, Y.; Fultz, B. Entropymetry of lithium intercalation in spinel manganese oxide: Effect of lithium stoichiometry. *ECS Trans.* **2006**, *1*, 87−96.
(19) Deng, J.; Bae, C.; Marcicki, J.; Masias, A.; Miller, T. Safety modelling and testing of lithium-ion batteries in electrified vehicles. *Nat. Energy* **2018**, *3*, 261−266.
(20) Jalkanen, K.; Vuorilehto, K. Entropy change characteristics of $LiMn_{0.67}Fe_{0.33}PO_4$ and $Li_4Ti_5O_{12}$ electrode materials. *J. Power Sources* **2015**, *273*, 351−359.
(21) Doh, C.-H.; Ha, Y.-C.; Eom, S.-w. Entropy measurement of a large format lithium ion battery and its application to calculate heat generation. *Electrochim. Acta* **2019**, *309*, 382−391.
(22) Shi, W.; Zheng, J.; Xiao, J.; Chen, X.; Polzin, B. J.; Zhang, J.-G. The effect of entropy and enthalpy changes on the thermal behavior of li-mn-rich layered composite cathode materials. *J. Electrochem. Soc.* **2016**, *163*, A571−A577.
(23) Xie, Y.; Shi, S.; Tang, J.; Wu, H.; Yu, J. Experimental and analytical study on heat generation characteristics of a lithium-ion power battery. *Int. J. Heat Mass Tran.* **2018**, *122*, 884−894.
(24) Honders, A.; Derkinderen, J.; Vanheeren, A.; Dewit, J.; Broers, G. The thermodynamic and thermoelectric properties of Li_xTiS_2 and Li_xCoO_2. *Solid State Ionics* **1984**, *14*, 205−216.
(25) Kobayashi, Y.; Mita, Y.; Seki, S.; Ohno, Y.; Miyashiro, H.; Nakayama, M.; Wakihara, M. Configurational entropy of lithium manganese oxide and related materials, $LiCr_yMn_{2-y}O_4$ (y=0, 0.3). *J. Electrochem. Soc.* **2008**, *155*, A14−A19.
(26) Baddour, R.; Pereira-Ramos, J. P.; Messina, R.; Perichon, J. A thermodynamic, structural and kinetic study of the electrochemical lithium intercalation into the xerogel $V_2O_5{\cdot}1.6H_2O$ in a propylene. *J. Electroanal. Chem.* **1991**, *314*, 81−101.
(27) Jalkanen, K.; Aho, T.; Vuorilehto, K. Entropy change effects on the thermal behavior of a $LiFePO_4$/graphite lithium-ion cell at different states of charge. *J. Power Sources* **2013**, *243*, 354−360.
(28) Tang, Y.; Wu, L.; Wei, W.; Wen, D.; Guo, Q.; Liang, W.; Xiao, L. Study of the thermal properties during the cyclic process of lithium ion power batteries using the electrochemical-thermal coupling model. *Appl. Therm. Eng.* **2018**, *137*, 11−22.
(29) Mao, J.; Tiedemann, W.; Newman, J. Simulation of temperature rise in li-ion cells at very high currents. *J. Power Sources* **2014**, *271*, 444−454.
(30) Pals, C. R.; Newman, J. Thermal modeling of the lithium/polymer battery i. Discharge behavior of a single cell. *J. Electrochem. Soc.* **1995**, *142*, 3274−3281.
(31) Zhu, J.; Wierzbicki, T.; Li, W. A review of safety-focused mechanical modeling of commercial lithium-ion batteries. *J. Power Sources* **2018**, *378*, 153−168.
(32) Yang, X.-G.; Liu, T.; Gao, Y.; Ge, S.; Leng, Y.; Wang, D.; Wang, C.-Y. Asymmetric temperature modulation for extreme fast charging of lithium-ion batteries. *Joule* **2019**, *3*, 3002.
(33) Julien, C. M.; Mauger, A. Review of 5-v electrodes for li-ion batteries: Status and trends. *Ionics* **2013**, *19*, 951−988.
(34) Dong, H.; Zhang, Y.; Zhang, S.; Tang, P.; Xiao, X.; Ma, M.; Zhang, H.; Yin, Y.; Wang, D.; Yang, S. Improved high temperature performance of a spinel $LiNi_{0.5}Mn_{1.5}O_4$ cathode for high-voltage lithium-ion batteries by surface modification of a flexible conductive nanolayer. *ACS Omega* **2019**, *4*, 185−194.
(35) Mao, J.; Dai, K.; Xuan, M.; Shao, G.; Qiao, R.; Yang, W.; Battaglia, V. S.; Liu, G. Effect of chromium and niobium doping on the morphology and electrochemical performance of high-voltage spinel lini0.5mn1.5o4 cathode material. *ACS Appl. Mater. Interfaces* **2016**, *8*, 9116−9124.
(36) Mao, J.; Ma, M.; Liu, P.; Hu, J.; Shao, G.; Battaglia, V.; Dai, K.; Liu, G. The effect of cobalt doping on the morphology and electrochemical performance of high-voltage spinel lini0.5mn1.5o4 cathode material. *Solid State Ionics* **2016**, *292*, 70−74.
(37) Komatsu, H.; Arai, H.; Koyama, Y.; Sato, K.; Kato, T.; Yoshida, R.; Murayama, H.; Takahashi, I.; Orikasa, Y.; Fukuda, K.; Hirayama, T.; Ikuhara, Y.; Ukyo, Y.; Uchimoto, Y.; Ogumi, Z. Solid solution domains at phase transition front of $Li_xNi_{0.5}Mn_{1.5}O_4$. *Adv. Energy Mater.* **2015**, *5*, 1500638.
(38) Manthiram, A.; Chemelewski, K.; Lee, E.-S. A perspective on the high-voltage $LiMn_{1.5}Ni_{0.5}O_4$ spinel cathode for lithium-ion batteries. *Energy Environ. Sci.* **2014**, *7*, 1339.
(39) Ma, J.; Hu, P.; Cui, G.; Chen, L. Surface and interface issues in spinel $LiNi_{0.5}Mn_{1.5}O_4$: Insights into a potential cathode material for high energy density lithium ion batteries. *Chem. Mater.* **2016**, *28*, 3578−3606.
(40) Zhang, X.-F.; Zhao, Y.; Patel, Y.; Zhang, T.; Liu, W.-M.; Chen, M.; Offer, G. J.; Yan, Y. Potentiometric measurement of entropy change for lithium batteries. *Phys. Chem. Chem. Phys.* **2017**, *19*, 9833−9842.
(41) Duncan, H.; Hai, B.; Leskes, M.; Grey, C. P.; Chen, G. Relationships between Mn^{3+} content, structural ordering, phase transformation, and kinetic properties in $LiNi_xMn_{2-x}O_4$ cathode materials. *Chem. Mater.* **2014**, *26*, 5374−5382.
(42) Mao, J.; Dai, K.; Zhai, Y. Electrochemical studies of spinel $LiNi_{0.5}Mn_{1.5}O_4$ cathodes with different particle morphologies. *Electrochim. Acta* **2012**, *63*, 381−390.

https://dx.doi.org/10.1021/acsomega.9b03794
ACS Omega 2020, 5, 4109−4114